Optimization of Protein-Ligand Electrostatic Interactions Using An Alchemical Free-Energy Method

Alexander D. Wade[a], David J. Huggins [a, b, c]

Affiliations: [a]TCM Group, Cavendish Laboratory, University of Cambridge, 19 J J Thomson Avenue, Cambridge CB3 0HE, United Kingdom

[b]Tri-Institutional Therapeutics Discovery Institute, Belfer Research Building, 413 East 69th Street, 16th Floor, Box 300, New York, USA

[c]Department of Physiology and Biophysics, Weill Cornell Medicine, 1300 York Avenue, New York, NY, 10065, USA.

Corresponding Author: David J. Huggins

Email: dhuggins@tritdi.org

Updated: 30th September 2019

ORCIDs: Alex Wade - 0000-0003-1500-3733

David Huggins 0000-0003-1579-2496

Abstract

We present an explicit solvent alchemical free-energy method for optimizing the partial charges of a ligand to maximize the binding affinity with a receptor. This methodology can be applied to known ligand-protein complexes to determine an optimized set of ligand partial atomic changes. Three protein-ligand complexes have been optimized in this work: FXa, P38 and the androgen receptor. The sets of optimized charges can be used to identify design principles for chemical changes to the ligands which improve the binding affinity for all three systems. In this work, beneficial chemical mutations are generated from these principles and the resulting molecules tested using free-energy perturbation calculations. We show that three quarters of our chemical changes are predicted to improve the binding affinity, with an average improvement for the beneficial mutations of approximately 1 kcal/mol. In the cases where experimental data is available, the agreement between prediction and experiment is also good. The results demonstrate that charge optimization in explicit solvent is a useful tool for predicting beneficial chemical changes such as pyridinations, fluorinations, and oxygen to sulphur mutations.

Introduction

In recent years, alchemical methods have garnered increasing attention in drug design [1–6]. In particular, free energy perturbation (FEP) is now commonly used by pharmaceutical companies due to improvements in efficiency [7], more accurate force fields [8,9] and increases in computational power. Based on the Zwanzig equation [10,11], it is common to use FEP calculations in drug design to calculate the relative binding affinity of two molecules [11–14]. This relative free energy, ΔG_{AB}, can be defined using the Zwanzig equation, as shown in Equation (1), as the free energy difference between thermodynamic states A and B.

$$\Delta G_{AB} = -kT ln < e^{-((E_B - E_A)/kT)} >_A \quad (1)$$

With k as Boltzmann's constant, T temperature, E_A and E_B as the potential energies of the system calculated using the Hamiltonian of state A and B and $< . >_A$ a state average over system A. Typically in free energy calculations Equation (1) is expanded upon to include sampling from both states A and B [15] or sampling from intermediate states [7]. This is done to improve the sampling overlap between end states. The drawback here is that for every relative binding affinity calculation, lengthy molecular dynamics (MD) simulations must be performed for all end and intermediate states. If, however, the perturbation between end states remains small enough, such that the overlap between end states is large, Equation (1) is sufficient without any intermediate states. Applying Equation (1) with no intermediate states is referred to as single step perturbation (SSP) and this is the primary free energy method used in this work. Numerous studies have used SSP [16–19], demonstrating that it is applicable to relative free energy calculations [20,21] and can be significantly faster than standard FEP [22]. Most recently, the authors of this paper have used SSP to perform computational fluorine scanning [23]. We now apply SSP with the goal of optimizing ligand partial charges.

Charge optimization was developed by Tidor and co-workers using an implicit water treatment of electrostatics [24,25]. Poisson-Boltzmann calculations are performed on the bound and unbound states in order to find the optimal partial charges of a given molecule [26–29]. This approach has since been used by other academic groups [30,31], employed in industry [32], and been extended to consider induced fit effects [33]. However, the approach suffers from the deficiencies of all implicit water approaches: it is unable to deal effectively with interfacial water molecules. These occur commonly and are very difficult to treat effectively with implicit solvent approaches. The accuracy of implicit water models is lacking for many types of free energy calculations [34–36], particularly relevant here are implicit model's shortcomings relative to explicit models for binding free energies [37]. Additionally, whilst previous work has considered flexibility in the ligand, the receptor and complex were assumed to be rigid. It is known that this may play a significant role in binding free energies [33]. Due to advances in available computing power, explicit water approaches to charge optimization are now possible. We propose to exploit these computational advances by applying SSP to the bound and unbound states of small molecule inhibitors to develop a method for electrostatic charge optimization in explicit solvent.

Combining SSP with explicit water MD calculations and flexible receptors and complexes has the potential to develop a more accurate charge optimizer. To carry out these charge optimizations, we developed a tool to automate their execution. This tool is freely available at https://github.com/adw62/Ligand_Charge_Optimiser. Our ligand charge optimizer uses OpenMM [38] as both an MD engine and a tool to create the modified alchemical systems. The software will generate all of the required mutant ligands from an input wild type ligand. These mutants are automatically parameterized, built into the complex systems, simulated, and optimized

Methods

We optimize the ligand partial charges for three protein test cases: FXa, P38 kinase, and the androgen receptor. The chemical structures of the ligands studied are shown

in Table (1). The ligands were built from highly related molecules in the Protein Databank [39]: 2RA0 [40] (FXa), 3S3I [41] (P38), and 2NW4 [42] (androgen receptor). These small modifications are made from the PDB to allow comparison with experimental data [40–42]. Superpositions of the molecules in the original PDB and the modified molecules are shown in Figures (S2-S4).

Table (1): Name of the target for each system with ligands 2D chemical structure and the PDBIDs of the target ligand complex.

Target	Ligand	PDBIDs
Factor Xa	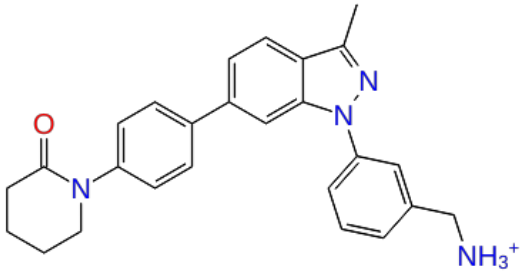	2RA0[40]
P38	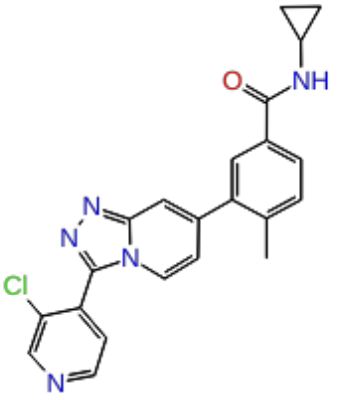	3S3I[41]
Androgen Receptor	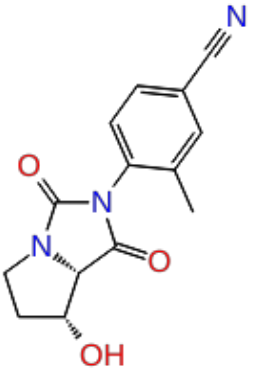	2NW4 [42]

System Setup

To prepare the Fxa, P38, and androgen receptor systems the non-standard residues were converted to their standard equivalents with pdbfixer [43]. Selenomethionines were changed to methionines and missing sidechains were added using Schrödinger's Preparation Wizard [44], which was also used to assign protonation state of all ionizable residues. All buffer solvents and ions were removed. The hydrogen atom positions were then built using tleap and force field parameters and partial charges were assigned from the AMBER ff14SB force field [9]. Parameters for the inhibitors were generated using Antechamber [45] with AMBER GAFF 2 [46] and AM1-BCC [47]. These structures and parameters were then passed to YANK's [48] 0.23.7 automatic setup pipeline to build solvated ligand-protein and ligand systems. For solvation, TIP4P-EW [49] was used. A salt concentration of 150 *mM* and any required counter-ions were added using sodium and chloride ions. In every case, the edge of the solvation box was set to be 15 *Å* from any atom of the receptor and ligand.

Molecular dynamics

MD sampling in this work is collected to compute SSP and FEP relative free energies, the amount of MD sampling varies for each application in this work and so is stated explicitly for each case in the relevant section. All simulations were performed with OpenMM 7.3.0 [43] as follows. First, OpenMM's default minimizer was used to minimize all structures. Then equilibration was performed in the NPT ensemble at 300 *k* and 1 *atm* using a Langevin integrator and Monte Carlo barostat for 250 *ps*. MD simulations were performed in the NPT ensemble using a time step of 2 *fs.* Van der Waals interactions were truncated at 11.0 *Å* with switching at 9.0 *Å*. Electrostatics were modeled using particle mesh Ewald method with a cutoff of 11.0 *Å*. All other simulation parameters were left as default. Snapshots were collected every 5 *ps* and all simulations were performed with constrained hydrogens.

Charge optimization

The objective function of this optimization was $\Delta G_{binding}(q_i) - \Delta G_{original}$. $\Delta G_{binding}(q_i)$ was defined as the difference in free energy between the bound and unbound states of the ligand and target for a ligand with charges q_i. $\Delta G_{original}$ was defined as the difference in free energy between the bound and unbound states of the ligand and target for a ligand with the charges of the original unoptimized ligand. $\Delta G_{original}$ is thus a constant. We therefore constructed the optimization problem as follows.

$$\min_{q_i} \quad \Delta G_{binding}(q_i) - \Delta G_{original} \tag{2}$$

$$\text{s.t.} \quad \sum_{i=1}^{m} q_i = net\ charge \tag{2.1}$$

$$\sqrt{\frac{\sum_{i=1}^{m} (q_{i,0} - q_{i,n+1})^2}{m}} \leq rmsd\ limit \tag{2.2}$$

$$|(q_{i,n} - q_{i,n+1})| \leq 0.01e \tag{2.3}$$

Where q_i are the charges of the ligand and $q_{i,n}$ the charges for iteration n of the optimization, m is the number of atoms in the ligand and $net\ charge$ the total net charge of the ligand. Equation (2.1) constrains the net charge of the ligand to be constant. Equation (2.2) constrains the root mean squared difference between the ligands original charges, $q_{i,0}$, and the $q_{i,n+1}$ charges to be less than some value $rmsd\ limit$. These $rmsd\ limits$ were chosen to limit the change in $\Delta\Delta G_{total}$ to a sensible range < 10 kcal/mol. Without this limit, the optimization continued to very large unphysical values of $\Delta\Delta G_{total}$ because atomic partial charges can reach unphysical values. The results of an unconstrained optimization can be seen in Figures (S17 - S19). Equation (2.3) constrains the perturbation to each atom to be less than 0.01 e per iteration, where e is the elementary charge. With this limit of 0.01 e a determination of how much sampling was required to give converged calculation of

$\Delta G_{binding}$ with a perturbation to each atom of 0.01 e was made in Figure (S14). The amount of sampling needed was determined to be 2.5 *ns*, this was then the amount of sampling used in this work to calculate the objective and gradient for each optimization step. The algorithm which was used to find a local minimum in this objective function was the SciPy 1.1.0 [50] implementation of the Sequential Least Squares Programming algorithm [51].

The primary calculations in this work were $\Delta\Delta G_{bindings}$ calculated as follows, first we applied SSP theory to calculate $\Delta G_{unperturbed->perturbed}$ in the bound and unbound states as shown in Equation (3).

$$\Delta G_{unperturbed->perturbed} = -kTln< e^{-((E_{perturbed}-E_{unperturbed})/kT)} >_{unperturbed} \quad (3)$$

$E_{perturbed}$ and $E_{unperturbed}$ are the potential energies of the system calculated using the Hamiltonian of the perturbed system and the unperturbed systems respectively. To change Hamatonians, the charges were switched from unperturbed to pertubed values, however, Lennard-Jones, bonded, angle and torsion parameters did not change. $\Delta\Delta G_{binding}$ was then constructed as shown in Equation (4). With $\Delta G^{bound}_{unperturbed->perturbed}$ and $\Delta G^{unbound}_{unperturbed->perturbed}$ as $\Delta G_{unperturbed->perturbed}$ calculated in the bound and unbound states of the ligand and target.

$$\Delta\Delta G_{binding} = \Delta G^{bound}_{unperturbed->perturbed} - \Delta G^{unbound}_{unperturbed->perturbed} \quad (4)$$

Note that $\Delta\Delta G_{binding}$ is equal to the objective function in equation 2 if we take equations 3-4 and set the $unperturbed$ state as the ligand with the original unoptimized charges and the $perturbed$ state as the ligand with charges q_i.

To calculate the gradient of the objective function in each direction in charge space a finite difference was calculated as shown in Equation (5).

$$\nabla(\Delta G_{binding}(q_i) - \Delta G_{original}) = \frac{\Delta G_{binding}(q_i+h) - \Delta G_{binding}(q_i)}{h} \quad (5)$$

Where h is a finite difference of 0.00015 e. The numerator of the RHS of Equation (5) is a $\Delta\Delta G_{binding}$ and can be calculated using an SSP approach as detailed in Equation (3, 4) where q_i are the $unperturbed$ charges and $q_i + h$ the $perturbed$ charges. This calculation of the gradient shows the advantage of SSP, as numerous (10s-100s) of evaluations of $\Delta\Delta G_{binding}$ are required, one for each direction in charge space. This $\Delta\Delta G_{binding}$ is between molecules that are extremely similar, differing only by 0.00015 e in one atom's partial charge. There is therefore likely to be a large sampling overlap between these states allowing SSP to be applied. Of note is that for each finite difference calculation the charge of the simulation box has been changed by 0.00015 e. The potential for finite size effects [52] caused by this change were investigated and the padding of the simulation with solvent chosen to negate these effects, see Figure (S15).

To delineate between the free energy change for individual optimization steps and the free energy change between the original and final optimized ligands, these will be defined as $\Delta\Delta G_{step}$ and $\Delta\Delta G_{total}$ respectively. Since an SSP method is being used, efforts were made to avoid poor overlap between the end states of any perturbations. To achieve this, the system was resampled after every optimization step. With the new sampling, the perturbed system could be redefined as a new unperturbed system after each optimization step. If this was not done then the difference between the perturbed and unperturbed systems would grow over the course of the optimization, reducing the overlap in sampling and so reducing the applicability of SSP. Resampling had an additional advantage as it allowed for a calculation of a reverse alchemical step. Therefore, $\Delta\Delta G_{step}$ for both the forwards and backwards alchemical transformation were calculated for every step and the $\Delta\Delta G_{step}$ in the results are reported as an average of the forwards and backwards transformations.

FEP Calculations

The optimization in this work gave a set of optimized charges and an associated $\Delta\Delta G_{binding}$ for going from the original set of ligand charges to the optimal set, named above as $\Delta\Delta G_{total}$. To validate the $\Delta\Delta G_{total}$ given by the optimization, we compared it against standard alchemical relative binding free energy calculations using the MBAR [7] estimator applied to the system with the original and optimized set of charges as end states. These calculations were run using the Ligand Charge Optimiser package as follows. For these calculations 12 equally spaced lambda windows (except when explicitly stated otherwise) were used. Between these windows the charge parameters were interpolated simultaneously from the original to optimized charges. All windows were sampled independently with 2 *ns* of Langevin dynamics totaling 24 *ns* of sampling. All simulation conditions were identical to the optimization MD calculations described above. The samples collected in each intermediate state were decorrelated based on an estimate of the statistical inefficiency of the reduced potentials time series before carrying out the MBAR analysis with the PyMBAR 3.0.1 [7].

In addition to testing the $\Delta\Delta G_{total}$ we also wished to calculate the $\Delta\Delta G_{binding}$ for a set of chemical changes informed by the optimal charges. This $\Delta\Delta G_{binding}$ is defined as $\Delta\Delta G_{designed}$ and is the change in binding free energy between the original ligand and a designed ligand with some chemical mutation. To perform these calculations, the protocol was the same for the full FEP calculation of $\Delta\Delta G_{total}$ but with the following additional considerations. Now, in addition to the charges, the van der Waals and bonded terms were all interpolated simultaneously from the original to the designed state. In the case of hydrogen to fluorine mutations the original hydrogen was constrained, therefore its associated C-H bond could not be interpolated to a C-F bond. When neglecting the interpolation of this bond the fluorine appeared at the position of the hydrogen, instead of the true physical position of the fluorine. To avoid this issue for fluorinations we used a hybrid topology approach where a massless interaction sites at the position of the mutation was added. This virtual site

represents the fluorine and its position was defined relative to the position of the parent hydrogen such that the C-F distance is always 1.24 times the C-H distance [53]. When mutating a hydrogen to fluorine, the relevant hydrogen was turned off and fluorine Lennard-Jones and charge parameters were applied to the additional site. When simulating these systems, all bonds to hydrogen were constrained. Since the position of the fluorine was defined relative to the position of its parent hydrogen it was also implicitly constrained. We therefore made the assumption that the C-F bond length oscillations were negligible. To prevent the hybrid topologies from interacting, the additional sites were excluded from interacting with their parent hydrogens.

Results

Using the optimization methodology above, the partial atomistic charges of three ligand-target systems are optimized. For each optimization, we would like to inspect the convergence over the number of steps. A good metric to analyse the results of the optimization is the set of optimized charges taken as a vector. In the methodology, mention was made to limiting the RMSD between the original and optimized charges to some value $rmsd\ limit$. The values which are chosen for $rmsd\ limit$ are 0.01, 0.03, and 0.05 e. The optimization is therefore repeated with the RMSD bound to these three values. With an RMSD bound of 0.01 e, the optimizer is limited to seven steps as adequate convergence is seen at this point. For a larger RMSD, the convergence is slower and therefore for optimizations with RMSD bounds of 0.03 and 0.05 e the optimizer is limited to 20 steps. To assess convergence across simulation steps, we take the dot product of the normalized vector of new charges with the normalized vector of original charges for each step of the optimization (see Figure (1)).

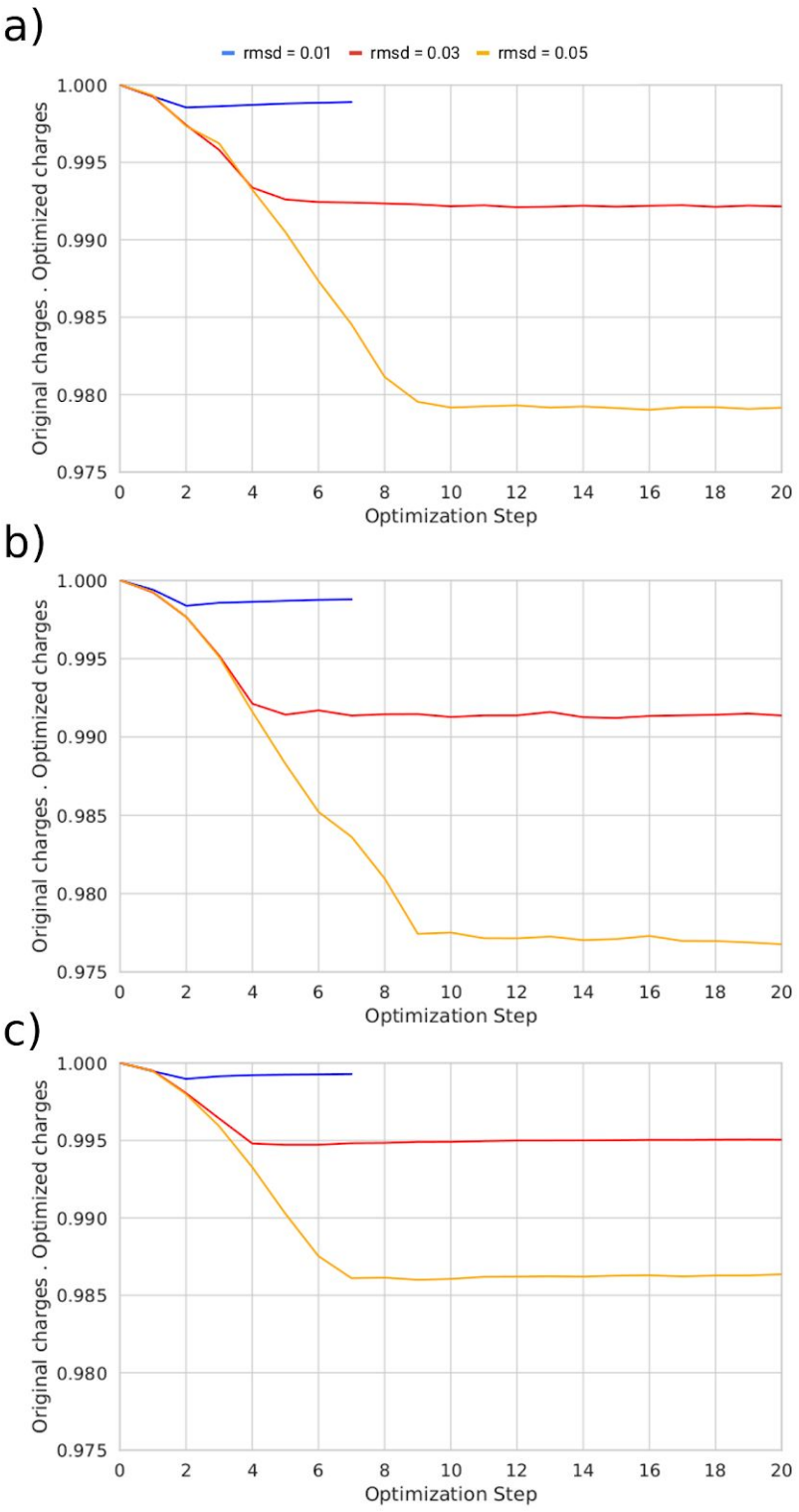

Figure (1) : Dot product of the normalized optimized charges with the normalized original charges showing variation of charge vector direction with step. Results are shown for RMSD limits 0.01, 0.03 and 0.05 e. With the FXa, P38 and androgen receptor systems labeled a), b) and c) respectively.

Figure (1) show that the direction of the charge vectors over all systems and RMSDs are well converged. The direction of these charge vectors represents where the charge is being applied on the molecule and this is the information that will be used in the following section to make chemical mutations to improve $\Delta\Delta G_{binding}$. It can also be seen that the dot product between the original and optimized charges is different for different RMSDs. To quantify this difference, the dot product between the set of optimal charges obtained for RMSD 0.01 with 0.03 and 0.05 e can be taken and the results of these projections can be seen in Table (2). Here we see that sets of charges for the same system are pointing in the same direction. Thus only the value of the charge changes are dependant on the RMSD, whilst the direction and relative magnitude of the charge changes are completely consistent. This is an important result because it shows that the design principles identified by the approach will not depend on the arbitrary choice of the RMSD. The invariance in where the charge is being applied can also be seen by eye if the atoms are colored by change in charge. Figures illustrating this are presented in the Figures (S5-S13) for all sets of optimized charge.

Table (2) : Dot products of the normalized vector of optimal charges using an RMSD of 0.01 q_e with the normalized vector of optimal charges using different RMSDs.

RMSD (e)	**FXa**	**P38**	**Androgen receptor**
0.01	1.00	1.00	1.00
0.03	1.00	1.00	1.00
0.05	0.99	0.98	0.99

In Table (2) we can see the dot product of the optimized charges from the optimization with an RMSD of 0.01 e with themselves returns 1.00 as expected. The dot product of the vector of charges with RMSD = 0.01 e with RMSD = 0.03 e also returns 1.00 as these vectors are extremely similar in direction. The dot product of the vector of charges with RMSD = 0.01 e with RMSD = 0.05 e returns

approximately 1.00 as these vectors are extremely similar in direction but not as close as 0.01 e with 0.03 e . To summarize, each optimization for a system added the charge in approximately the same place. It is only the magnitude of this charge that varies with RMSD. We can also look at the convergence of $\Delta\Delta G_{step}$ with optimisation step and this can be seen in Figure (2).

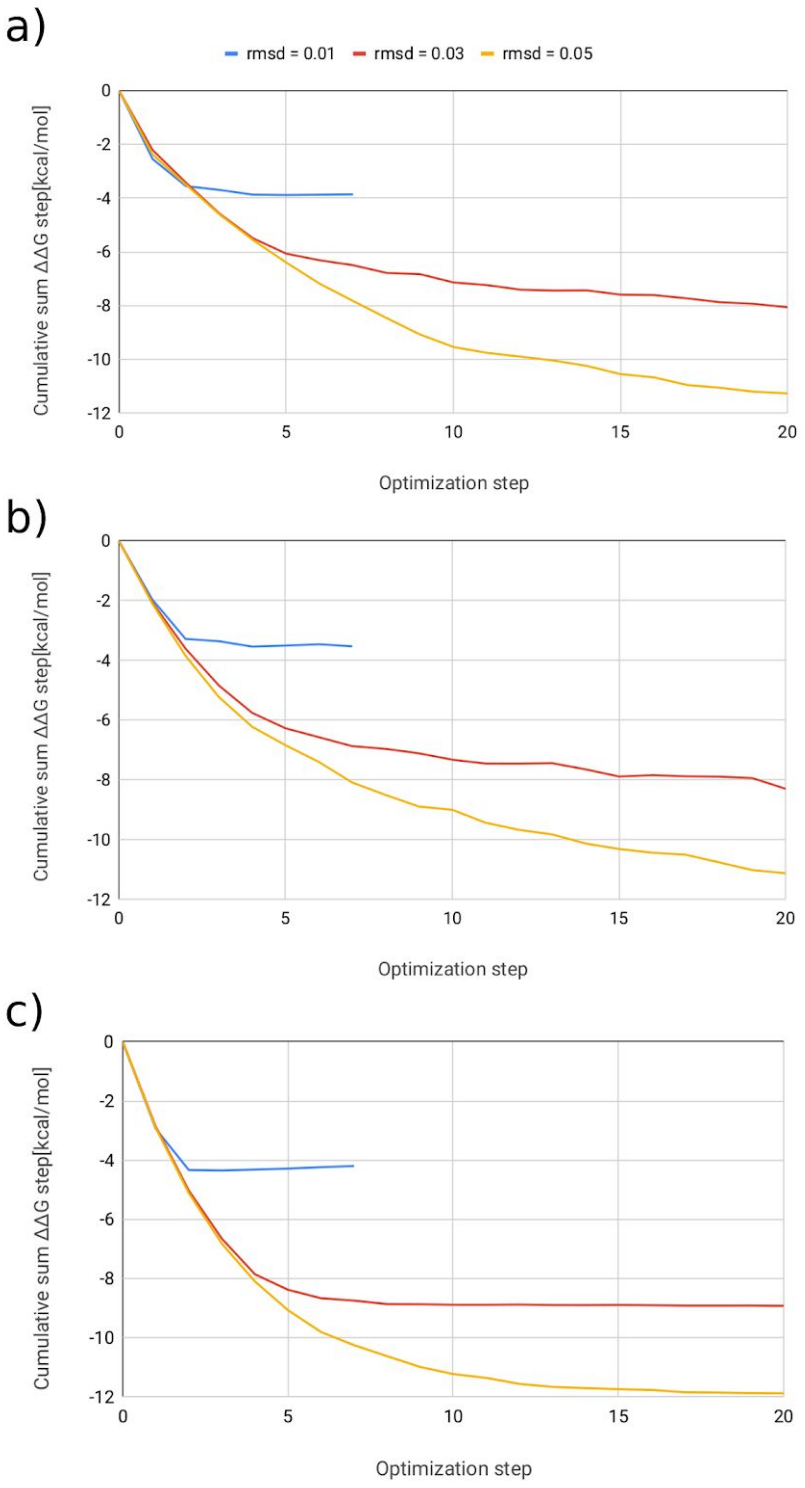

Figure (2): Cumulative sum of $\Delta\Delta G_{step}$ averaged over three replicates for each step of the optimizer. Three optimizations are shown with RMSD bound to 0.01, 0.03 and 0.05 e. With the FXa, P38 and androgen receptor systems labeled a), b) and c) respectively.

With an RMSD of 0.01 e Figure (2) demonstrates that $\Delta\Delta G_{step}$ is well converged for all systems. For a RMSDs of 0.03 or 0.05 e the results are only well-converged for the androgen receptor system, Figure (2c). This suggests that $\Delta\Delta G_{step}$ for the optimized set of charges is dependant on the RMSD and $\Delta\Delta G_{step}$ is slow to converge for larger ligands such as those in the p38 and FXa test cases. $\Delta\Delta G_{total}$ can be calculated between the original and the optimized charges with the cumulative sum of the SSP $\Delta\Delta G_{step}$ for all optimization step. This gives a $\Delta\Delta G_{total}$ that will be termed as the $\Delta\Delta G_{total}^{SSP}$. We compare this SSP $\Delta\Delta G_{total}$ for each set of optimized charges with full FEP calculations, see Table (3). These FEP calculations use the original and optimized charges as the two end states and the resulting $\Delta\Delta G_{total}$ will be termed as the $\Delta\Delta G_{total}^{FEP}$.

Table (3): Calculated $\Delta\Delta G_{total}$ for the set of optimal charges. SSP $\Delta\Delta G_{total}$ values are calculated by summing the average of forward and backwards SSP calculations made for each step of the optimizer. FEP $\Delta\Delta G_{total}$ values are calculated from an alchemical transformation from the original charges to the optimal charges. SSP and FEP predictions are reported as the mean of three replicates with 95% confidence interval reported between square brackets computed as mean ± t2 · SEM, where t2 is the t-distribution statistic with two degrees of freedom, and SEM is the standard error of the mean computed from the sample standard deviation of the three independent replicate predictions.

FXa			
RMSD (e)	**0.05**	**0.03**	**0.01**
$\Delta\Delta G_{total}^{FEP}$ [kcal/mol]	-8.7 [-9.2, -8.2]	-6.3 [-6.5, -6.1]	-3.1 [-3.4, -2.9]
$\Delta\Delta G_{total}^{SSP}$ [kcal/mol]	-11.3 [-12.4, -10.1]	-8.1 [-9.1, -7.0]	-3.9 [-4.4, -3.3]

P38			
RMSD (e)	**0.05**	**0.03**	**0.01**
$\Delta\Delta G_{total}^{FEP}$ [kcal/mol]	-9.4 [-10.8, -8.0]	-6.6 [-7.2, -6.0]	-3.2 [-3.4, -3.1]
$\Delta\Delta G_{total}^{SSP}$ [kcal/mol]	-11.1 [-11.5, -10.8]	-8.3 [-8.7, -7.9]	-3.5 [-4.0, -3.1]
Androgen Receptor			
RMSD (e)	**0.05**	**0.03**	**0.01**
$\Delta\Delta G_{total}^{FEP}$ [kcal/mol]	-11.5 [-12.0, -10.9]	-8.8 [-8.8, -8.8]	-4.2 [-4.2, -4.1]
$\Delta\Delta G_{total}^{SSP}$ [kcal/mol]	-11.9 [-12.3, -11.5]	-8.9 [-9.2, -8.7]	-4.2 [-4.4, -4.0]

Table (3) shows that the SSP and FEP calculations are well agreed with an RMSD of 0.01 e (differing by less than 1.0 kcal/mol in all cases). For an RMSD of 0.03 and 0.05 e, SSP and FEP are less well agreed (differing by more than 1.0 kcal/mol in some cases). Table (3) also shows clearly that changing the RMSD changes the calculated $\Delta\Delta G_{total}$. The relation here is that increasing the RMSD bound increases how much the charges can be changed and so increases the change in $\Delta\Delta G_{total}$. However, as discussed above, the convergence of $\Delta\Delta G_{total}$ is an unnecessary condition, providing no additional information. It is only critical that the direction of the charge vectors are well converged and consistent for all RMSD values for all test cases, which as been shown in Figure (1) and Table (2), as it is this information that will inform what chemical mutations are proposed for the ligands. As such we then use where the optimiser has placed the charge as a design tool to generate ideas for beneficial chemical mutations and this is presented in Figure (3).

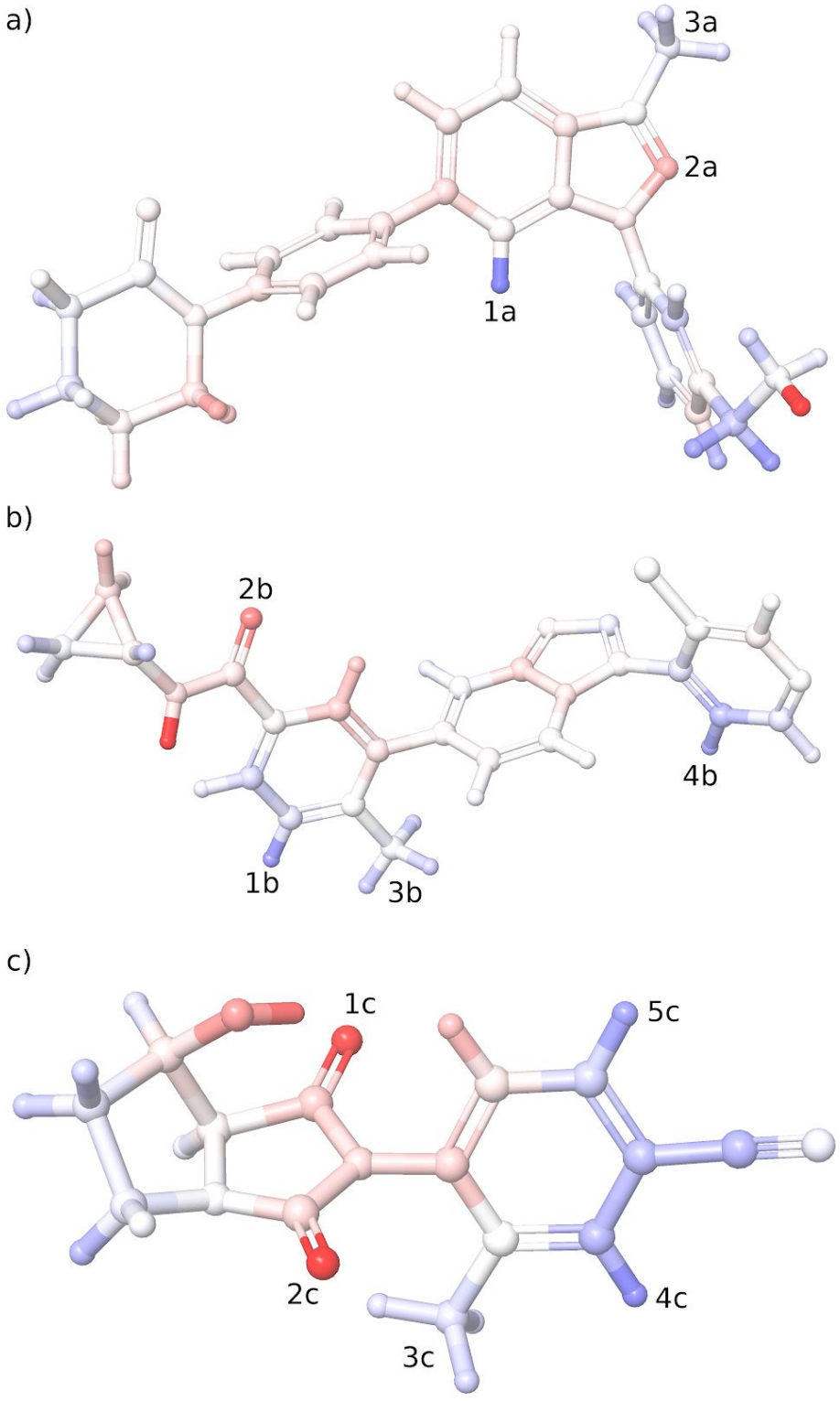

Figure (3): Panels a), b) and c) show the FXa, P38 and androgen receptor ligands with atoms coloured by change in charge relative to the original partial charges. The optimised charge is taken from the optimisation with RMSD bound to 0.03 e. Blue represents atoms which are more negative and red represents atoms which are more positive. Selected sites for chemical modification are numbered.

We developed specific design ideas to improve $\Delta\Delta G_{binding}$ based on the changes in charge. First analyzing the Fxa ligand, three options are selected:

- Replacing the hydrogen with a fluorine at position 1a.
- Replacing the nitrogen with a carbon at position 2a.
- Replacing one or more of the hydrogens with a fluorine atom on the methyl group at position 3a.

Analyzing the P38 ligand, four options are selected:

- Replacing the hydrogen with a fluorine at position 1b or 4b.
- Replacing the nitrogen with a carbon at position 1b or 4b.
- Replacing the oxygen with a sulphur at position 2b .
- Replacing one or more of the hydrogens with a fluorine atom on the methyl group at position 3b.

The final set of changes apply to the ligand of the androgen receptor with three options selected:

- Replacing the oxygen with a sulphur at position 1c and 2c
- Replacing the hydrogen with a fluorine at position 3c, 4c or 5c.
- Replacing the bonded carbon with a nitrogen at positions 4c or 5c.

$\Delta\Delta G_{designed}$ for all of these changes was calculated using the FEP protocol discussed in the methods section. Each FEP calculation was performed in triplicate and the averaged results of these calculations can be seen in Table (4).

Table (4): $\Delta\Delta G_{designed}$ for proposed chemical mutations to the FXa, P38 and androgen receptor ligands calculated with FEP. The positions denoted numerically corresponds to numerical positions in Figure (3). 2D structures of the mutation are presented in the column labeled mutant. FEP predictions are reported as the mean

value of three replicates with 95% confidence interval reported between square brackets computed as mean ± t2 · SEM, where t2 is the t-distribution statistic with two degrees of freedom, and SEM is the standard error of the mean computed from the sample standard deviation of the three independent replicate predictions. The asterisk label * indicates single or double fluorinations of a methyl. These are averaged over every hydrogen or pair of hydrogen in the methyl and as such this data represents the averaging of nine replicates with the confidence interval reported such that t2 is now the t-distribution statistic with eight degrees of freedom. The obelisk label † denotes calculations that were slow to converge and run with 24 lambda windows of 2ns. The diesis ‡ label denotes data taken from previous work of the authors [23].

FXa		
Position and mutation	**Mutant**	**FEP $\Delta\Delta G_{designed}$ [kcal/mol]**
(1a) Hydrogen to fluorine	1. 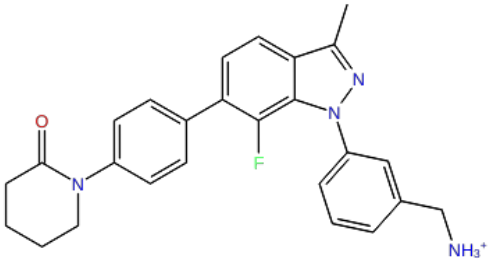	-2.2 [-2.3, -2.1]‡
(2a) Nitrogen to carbon	2. 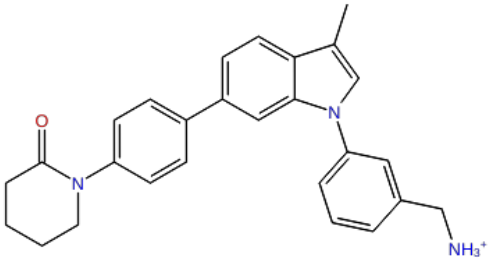	3.0 [1.9, 4.1]
(3a) Hydrogen to fluorine	3. 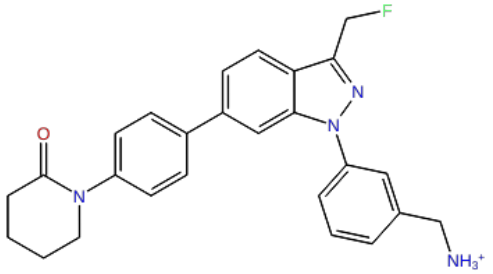	-0.1 [-0.2, 0.0]*

(3a) Double hydrogen to fluorine	4. 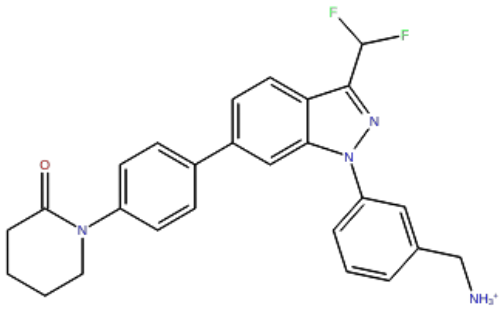	-0.6 [-0.7, -0.5]*
(3a) Triple hydrogen to fluorine	5. 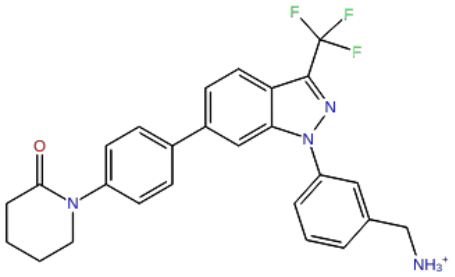	-0.8 [-1.2, -0.5]
P38		
Position	**Mutant**	**FEP $\Delta\Delta G_{designed}$ [kcal/mol]**
(1b) Hydrogen to fluorine	6. 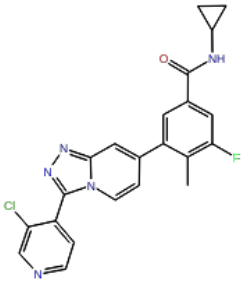	-2.2 [-2.7, -1.6]‡
(1b) Carbon to nitrogen	7. 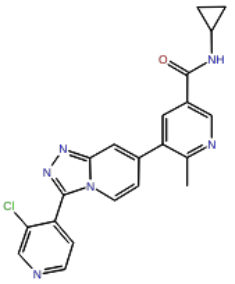	2.0 [1.2, 2.7]
(2b) Oxygen to sulphur	8.. 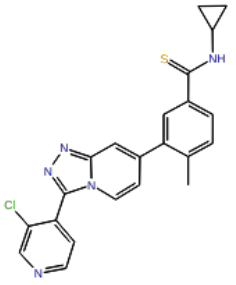	0.0 [-2.7 , 2.7]†

(3b) Hydrogen to fluorine	9. 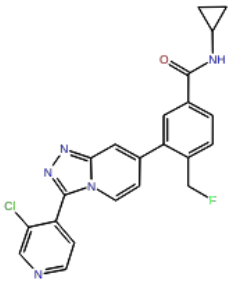	0.3 [0.1, 0.4]*
(3b) Double hydrogen to fluorine	10. 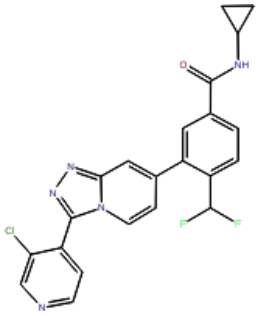	-0.5 [-0.9, -0.1]*
(3b) Triple hydrogen to fluorine	11. 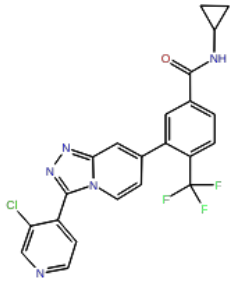	1.0 [-0.1, 2.1]
(4b) Hydrogen to fluorine	12. 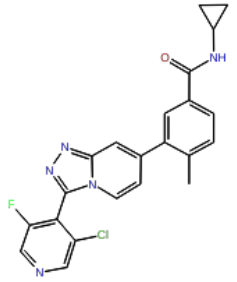	-1.6 [-1.7, -1.4]‡
(4b) Carbon to nitrogen	13. 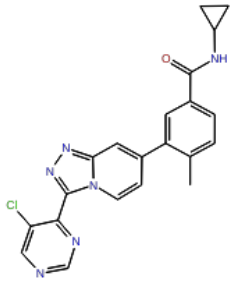	-0.4 [-1.7, 1.0]
<u>Androgen Receptor</u>		
Position	**Mutant**	**FEP $\Delta\Delta G_{designed}$ [kcal/mol]**

(1c) Oxygen to sulphur	14. 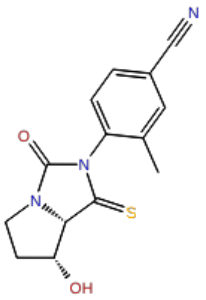	-2.1 [-3.3 , -0.9]
(2c) Oxygen to sulphur	15. 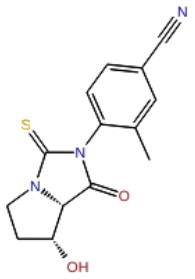	-2.0 [-3.2 , -0.8]
(3c) Hydrogen to fluorine	16. 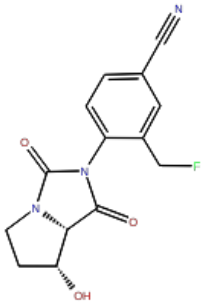	-0.6 [-0.8, -0.4]*
(3c) Double hydrogen to fluorine	17. 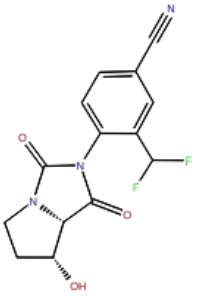	-1.6 [-1.8 , -1.4]*
(3c) Triple hydrogen to fluorine	18. 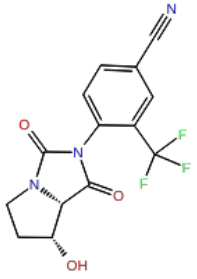	-0.1 [-0.9, 1.0]

(4c) Hydrogen to fluorine	19. 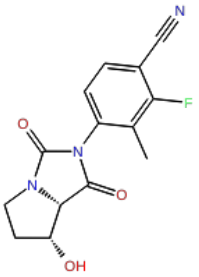	-2.5 [-2.8, -2.1]‡
(4c) Carbon to nitrogen	20. 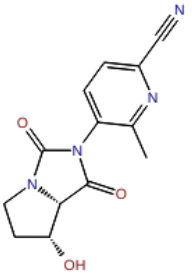	-0.9 [-1.4, -0.5]
(5c) Hydrogen to fluorine	21. 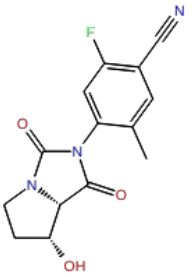	-0.3 [-0.3, -0.2]‡
(5c) Carbon to nitrogen	22. 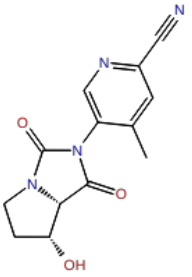	1.1 [0.0, 2.2]

The atoms indicated by the optimization to beneficially be more negative in Figure (3) line up with experimental work on these test cases [40–42]. Mutants 1, 6, and 19 are predicted by FEP to be beneficial (-2.2 kcal/mol, -2.2 kcal/mol, and -2.5 kcal/mol respectively) and this is in good agreement with experimental data (-2.1 kcal/mol, -2.3 kcal/mol, and -1.1 kcal/mol respectively). Experimental data does not exist for the remaining proposed mutations. However, 73% of the mutations in Table (6) are predicted to be favourable by FEP. Both the FXa and androgen systems have a higher success rate with 80% and 89% of ideas from charge optimization being

beneficial as assessed by FEP respectively. P38 has a lower (though still promising) success rate with 50% of mutations being beneficial as assessed by FEP.

Conclusions

We have demonstrated ligand charge optimization in explicit solvent to be a useful tool to rationally design ligands with improved binding affinities. The electrostatics of three ligand receptor systems were systematically optimized using the alchemical SSP method, yielding sets of optimal ligand charges. These sets of optimal charges were used to generate design principles for chemical mutations to the ligands that would yield improved receptor binding affinity. These chemical mutations were assessed with a more rigorous FEP method. Using FEP, 73% of the predicted chemical mutations were found to be beneficial. The average improvement of the beneficial mutations was approximately 1 kcal/mol. In three of these cases, experimental data exists and is in excellent agreement with calculations, with mutants 1, 6, and 19 in Table (4) predicted by FEP to be beneficial (-2.2 kcal/mol, -2.2 kcal/mol, and -2.5 kcal/mol respectively) compared to the experimental data (-2.1 kcal/mol, -2.3 kcal/mol, and -1.1 kcal/mol respectively).

The major advantage of SSP shown in this work is the calculation of the gradient. SSP allows for many highly related mutations to be assessed quickly, as is required to calculate the gradient via a finite difference method. For comparison, to collect 2.5 *ns* of sampling for the FXa system with 99, 000 and 13, 000 atoms in the complex and solvent systems respectively takes 29 minutes. To calculate a gradient from this sampling takes 15 minutes and so, including sampling, this totals to 44 minutes per gradient. To calculate a perturbation 0.00015 e of with full FEP (assuming 1.0 *ns* of sampling converges $\Delta\Delta G_{binding}$, see Figure (S16) for convergence plot) takes 14 minutes. With 58 charges in the FXa ligand, which must all be perturbed in the complex and solvent systems, this gives approximately 27 hours to calculate one gradient. This advantage would only be compounded if a more complex optimization scheme, which required a calculation of the Hessian, was used. Both these

calculations of the gradient are run in parallel (see Supporting Information for parallelization strategy) across 4 NVIDIA P100 GPUs using OpenMM 7.3.0 and CUDA 10.0.

This ligand charge optimization methodology could be easily extended by considering the optimization of any other parameter of the force field with respect to the binding free energy. For example, the van der Waals parameters could be 'optimized'. Additionally, the calculation for the gradient of force field parameters with respect to potential energies could be used in the systematic optimization of a small molecule force field. Since here we have demonstrated a methodology for quickly calculating gradients of force field parameters with respect to free energy this could lead to some interesting studies of force field optimization using experimental ligand-receptor binding energies as a target data set. This method is relatively unique in providing drug design principles from alchemical free-energy calculations along with a rationale for increases or decreases in binding due to specific changes to the ligand [54].

In summary, we have presented a novel technique for identifying partial charges that optimize protein-ligand binding affinities and highlighted ways in which these predictions can be turned into design principles for drug discovery. The method is fast compared to traditional FEP, easy to interpret, and simple to test by using more thorough approaches such as MBAR.

Supporting Information

Figure (S1) 3D structures of ligands with all atoms named. Figures (S2-S4) showing superposition of ligands in PDBs and manually built ligands used in this work. Table (S1) contains original charges of ligands used in this work. Table (S2) contains optimised charges for all optimizations. Figures (S5-S13) show ligands colored by all set of optimised charges. Figure (S14) convergence plot for $\Delta\Delta G$ with sampling time calculated using SSP. Figure (S15) convergence plot for ΔG with box size calculated using SSP. Figure (S16) convergence plot for $\Delta\Delta G$ with sampling time calculated using full FEP. Figure (S17) shows FXa ligand colored by a set of optimised charges from an optimization with no rmsd constraint. Figure (S18) $\Delta\Delta G$ plotted against step from an optimization for FXa with no rmsd constraint. Figure (S19) Dot product of the normalized optimized charges with the normalized original charges showing variation of charge vector direction with step for FXa with no rmsd constraint. Discussion of parallelization strategy for all calculations.

Acknowledgments: The authors would like to thank Andrea Rizzi, Yuanqing Wang, and John Chodera for useful discussions. A.D.W. would like to acknowledge the EPSRC Centre for Doctoral Training in Computational Methods for Materials Science for funding under grant number EP/L015552/1. A.D.W would also like to acknowledge Michael Hutcheon and Nick Woods for enlightening discussions and suggestions that are reflected in this manuscript. All calculations were performed using the Darwin Supercomputer of the University of Cambridge High Performance Computing Service (http://www.hpc.cam.ac.uk/) and were funded by the EPSRC under grant EP/P020259/1.

Notes: The authors declare the following competing financial interest(s): D.H. is a founder and shareholder of Integrated Biomedical Solutions Ltd.

Table of contents graphic:

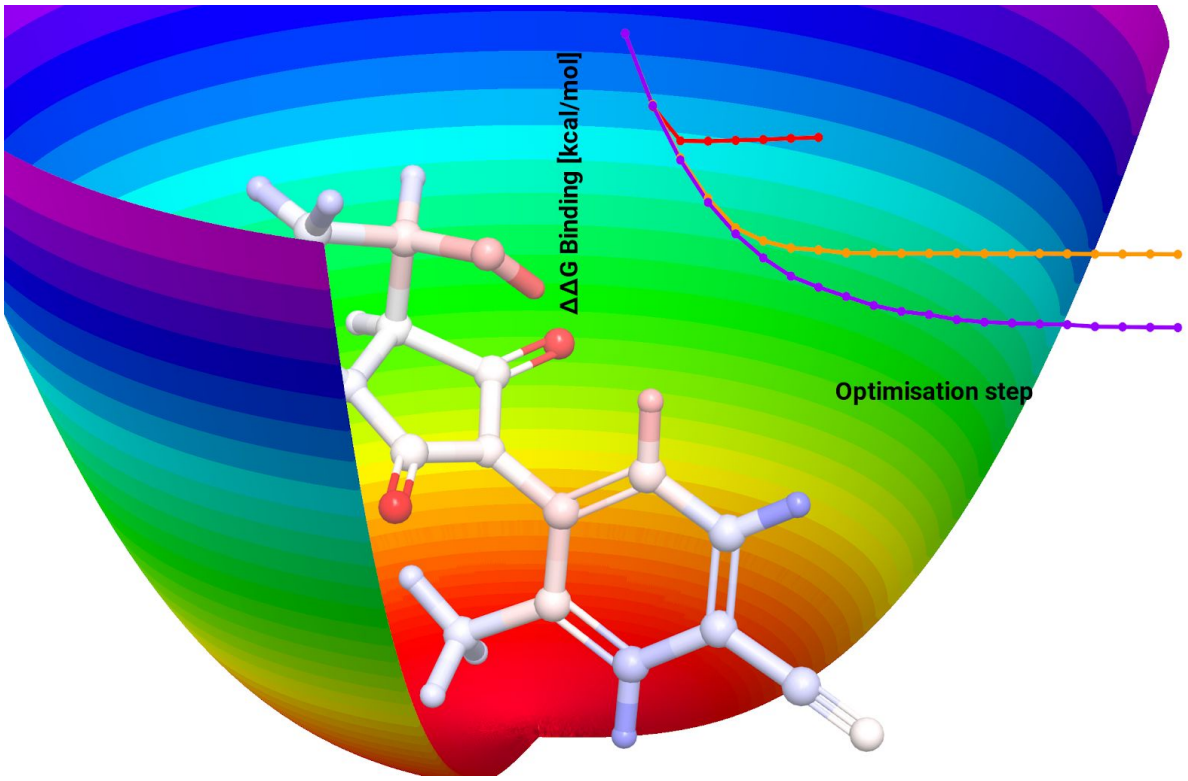

References

(1) Wang, L.; Wu, Y.; Deng, Y.; Kim, B.; Pierce, L.; Krilov, G.; Lupyan, D.; Robinson, S.; Dahlgren, M. K.; Greenwood, J.; Romero, D.L. Accurate and Reliable Prediction of Relative Ligand Binding Potency in Prospective Drug Discovery by Way of a Modern Free-Energy Calculation Protocol and Force Field. *J. Am. Chem. Soc.* **2015**, 137, 2695–2703.

(2) Williams-Noonan, B. J.; Yuriev, E.; Chalmers, D. K. Free Energy Methods in Drug Design: Prospects of "alchemical Perturbation" in Medicinal Chemistry: Miniperspective. *J. Med. Chem.* **2017**, *61*, 638–649.

(3) Seeliger, D.; de Groot, B. L. Protein Thermostability Calculations Using Alchemical Free Energy Simulations. *Biophys. J.* **2010**, *98*, 2309–2316.

(4) Loeffler, H. H.; Michel, J.; Woods, C. FESetup: Automating Setup for Alchemical Free Energy Simulations. *J. Chem. Inf. Model.* **2015**, *55*, 2485–2490.

(5) Cournia, Z.; Allen, B.; Sherman, W. Relative Binding Free Energy Calculations in Drug Discovery: Recent Advances and Practical Considerations. *J. Chem. Inf. Model.* **2017**, *57*, 2911–2937.

(6) Cole, D. J.; Tirado-Rives, J.; Jorgensen, W. L. Molecular Dynamics and Monte Carlo Simulations for Protein–ligand Binding and Inhibitor Design. *Biochim. Biophys. Acta.* **2015**, *1850*, 966–971.

(7) Shirts, M. R.; Chodera, J. D. Statistically Optimal Analysis of Samples from Multiple Equilibrium States. *J. Chem. Phys.* **2008**, *129*, 124105.

(8) Roos, K.; Wu, C.; Damm, W.; Reboul, M.; Stevenson, J. M.; Lu, C.; Dahlgren, M. K.; Mondal, S.; Chen, W.; Wang, L.; Abel, R. OPLS3e: Extending Force Field Coverage for Drug-Like Small Molecules. *J. Chem. Theory Comput.* **2019**, 15, 1863-1874.

(9) Maier, J. A.; Martinez, C.; Kasavajhala, K.; Wickstrom, L.; Hauser, K. E.; Simmerling, C. ff14SB: Improving the Accuracy of Protein Side Chain and Backbone Parameters from ff99SB. *J. Chem. Theory Comput.* **2015**, *11*, 3696–3713.

(10) Zwanzig, R. W. Erratum : High-Temperature Equation of State by a Perturbation Method. I. Nonpolar Gases. *J. Chem. Phys*. **1954**, 22, 1420-1426.

(11) Abel, R.; Wang, L.; Harder, E. D.; Berne, B. J.; Friesner, R. A. Advancing Drug Discovery through Enhanced Free Energy Calculations. *Acc. Chem. Res.* **2017**, *50*, 1625–1632.

(12) Chodera, J. D.; Mobley, D. L.; Shirts, M. R.; Dixon, R. W.; Branson, K.; Pande, V. S. Alchemical Free Energy Methods for Drug Discovery: Progress and Challenges. *Curr. Opin. Struct. Biol.* **2011**, *21*, 150–160.

(13) Lybrand, T. P.; McCammon, J. A.; Wipff, G. Theoretical Calculation of Relative Binding Affinity in Host-Guest Systems. *Proc. Natl. Acad. Sci. U.S.A.* **1986**, *83*, 833–835.

(14) Cole, D. J.; Janecek, M.; Stokes, J. E.; Rossmann, M.; Faver, J. C.; McKenzie, G. J.; Venkitaraman, A. R.; Hyvönen, M.; Spring, D. R.; Huggins, D. J.; Jorgensen, W.L. Computationally-Guided Optimization of Small-Molecule Inhibitors of the Aurora A kinase–TPX2 Protein–protein Interaction. *Chem. Commun*. **2017,** 9372–9375.

(15) Shirts, M. R.; Pande, V. S. Comparison of Efficiency and Bias of Free Energies Computed by Exponential Averaging, the Bennett Acceptance Ratio,

and Thermodynamic Integration. *J. Chem. Phys.* **2005**, *122*, 144107.
(16) Liu, H.; Mark, A. E.; van Gunsteren, W. F. Estimating the Relative Free Energy of Different Molecular States with Respect to a Single Reference State. *J. Phys. Chem.* **1996**, *100*, 9485–9494.
(17) Mordasini, T. Z.; Andrew McCammon, J. Calculations of Relative Hydration Free Energies: A Comparative Study Using Thermodynamic Integration and an Extrapolation Method Based on a Single Reference State. *J. Phys. Chem. B*. **2000,** 360–367.
(18) Raman, E. P.; Prabhu Raman, E.; Vanommeslaeghe, K.; MacKerell, A. D. Site-Specific Fragment Identification Guided by Single-Step Free Energy Perturbation Calculations. *J. Chem. Theory Comput*. **2012**, 3513–3525.
(19) Stroet, M.; Koziara, K. B.; Malde, A. K.; Mark, A. E. Optimization of Empirical Force Fields by Parameter Space Mapping: A Single-Step Perturbation Approach. J. Chem. Theory Comput.. **2017**, 6201–6212.
(20) Oostenbrink, C.; Van Gunsteren, W. F. Single-Step Perturbations to Calculate Free Energy Differences from Unphysical Reference States: Limits on Size, Flexibility, and Character. *J. Comp. Chem*. **2003,** 1730–1739.
(21) Oostenbrink, C.; van Gunsteren, W. F. Free Energies of Ligand Binding for Structurally Diverse Compounds. *Proc. Natl. Acad. Sci. U.S.A.* **2005**, *102*, 6750–6754.
(22) Raman, E. P.; Prabhu Raman, E.; Lakkaraju, S. K.; Denny, R. A.; MacKerell, A. D. Estimation of Relative Free Energies of Binding Using Pre-Computed Ensembles Based on the Single-Step Free Energy Perturbation and the Site-Identification by Ligand Competitive Saturation Approaches. *J. Comp. Chem*. **2017**, 1238–1251.
(23) Wade, A. D.; Rizzi, A.; Wang, Y.; Huggins, D. J. Computational Fluorine Scanning Using Free-Energy Perturbation. *J. Chem. Inf. Model.* **2019**.
(24) Lee, L.-P.; Tidor, B. Optimization of Electrostatic Binding Free Energy. *J. Chem. Phys.* **1997**, *106*, 8681–8690.
(25) Kangas, E.; Tidor, B. Charge Optimization Leads to Favorable Electrostatic Binding Free Energy. *Phys. Rev. E Stat. Phys. Plasmas Fluids Relat. Interdiscip. Topics* **1999**, *59*, 5958–5961.
(26) Kangas, E.; Tidor, B. Electrostatic Specificity in Molecular Ligand Design. *J. Chem. Phys.* **2000**, *112*, 9120–9131.
(27) Lee, L. P.; Tidor, B. Optimization of Binding Electrostatics: Charge Complementarity in the Barnase-barstar Protein Complex. *Protein Sci.* **2001**.
(28) Bardhan, J. P.; Lee, J. H.; Kuo, S. S.; Altman, M. D.; Tidor, B.; White, J. K. Fast Methods for Biomolecule Charge Optimization. *Modeling and Simulation of Microsystems (Nanotech)* **2003**.
(29) Kangas, E.; Tidor, B. Electrostatic Complementarity at Ligand Binding Sites: Application to Chorismate Mutase. *J. Phys. Chem. B* **2001**, *105* (4), 880–888.
(30) Sims, P. A.; Wong, C. F.; McCammon, J. A. Charge Optimization of the Interface between Protein Kinases and Their Ligands. *J. Comput. Chem.* **2004**, *25*, 1416–1429.
(31) Sulea, T.; Purisima, E. O. Optimizing Ligand Charges for Maximum Binding Affinity. A Solvated Interaction Energy Approach. *J. Phys. Chem. B* **2001**, *105*, 889–899.
(32) Armstrong, K. A.; Tidor, B.; Cheng, A. C. Optimal Charges in Lead

Progression: A Structure-Based Neuraminidase Case Study. *J. Med. Chem.* **2006**, *49*, 2470–2477.
(33) Shen, Y.; Gilson, M. K.; Tidor, B. Charge Optimization Theory for Induced-Fit Ligands. *J. Chem. Theory Comput.* **2012**, *8*, 4580–4592.
(34) Zhang, J.; Zhang, H.; Wu, T.; Wang, Q.; van der Spoel, D. Comparison of Implicit and Explicit Solvent Models for the Calculation of Solvation Free Energy in Organic Solvents. *J. Chem. Theory Comput.* **2017**, *13*, 1034–1043.
(35) Harris, R. C.; Pettitt, B. M. Examining the Assumptions Underlying Continuum-Solvent Models. *J. Chem. Theory Comput.* **2015**, *11*, 4593–4600.
(36) Zhang, H.; Tan, T.; van der Spoel, D. Generalized Born and Explicit Solvent Models for Free Energy Calculations in Organic Solvents: Cyclodextrin Dimerization. *J. Chem. Theory Comput.* **2015**, *11*, 5103–5113.
(37) Zhang, H.; Yin, C.; Yan, H.; van der Spoel, D. Evaluation of Generalized Born Models for Large Scale Affinity Prediction of Cyclodextrin Host–Guest Complexes. *J. Chem. Inf. Model.* **2016**, *56*, 2080–2092.
(38) Eastman, P.; Friedrichs, M. S.; Chodera, J. D.; Radmer, R. J.; Bruns, C. M.; Ku, J. P.; Beauchamp, K. A.; Lane, T. J.; Wang, L.-P.; Shukla, D.; Tye, T. OpenMM 4: A Reusable, Extensible, Hardware Independent Library for High Performance Molecular Simulation. *J. Chem. Theory Comput.* **2013**, *9*, 461–469.
(39) Berman, H. M.; Westbrook, J.; Feng, Z. The Protein Data Bank. *Nucleic acids* **2000**, 28, 235-242.
(40) Lee, Y.-K.; Parks, D. J.; Lu, T.; Thieu, T. V.; Markotan, T.; Pan, W.; McComsey, D. F.; Milkiewicz, K. L.; Crysler, C. S.; Ninan, N.; Abad, M.C. 7-Fluoroindazoles as Potent and Selective Inhibitors of Factor Xa†. *J. Med. Chem*. **2008**, 282–297.
(41) Aiguadé, J.; Balagué, C.; Carranco, I.; Caturla, F.; Domínguez, M.; Eastwood, P.; Esteve, C.; González, J.; Lumeras, W.; Orellana, A.; Preciado, S. Novel Triazolopyridylbenzamides as Potent and Selective p38α Inhibitors. *Bioorg. Med. Chem. Lett.* **2012**, *22*, 3431–3436.
(42) Hamann, L. G.; al., E. al et. Tandem Optimization of Target Activity and Elimination of Mutagenic Potential in a Potent Series of N-Aryl Bicyclic Hydantoin-Based Selective Androgen Receptor Modulators. *ChemInform*. **2007**, *17*, 1860-1864.
(43) Eastman, P.; Swails, J.; Chodera, J. D. OpenMM 7: Rapid Development of High Performance Algorithms for Molecular Dynamics. *PLoS Comput. Biol.* **2017**, *13*, e1005659.
(44) Sastry, G. M.; Adzhigirey, M.; Day, T.; Annabhimoju, R.; Sherman, W. Protein and Ligand Preparation: Parameters, Protocols, and Influence on Virtual Screening Enrichments. *J. Comput. Aided Mol. Des.* **2013**, *27*, 221–234.
(45) Wang, J.; Wang, W.; Kollman, P. A.; Case, D. A. Antechamber: An Accessory Software Package for Molecular Mechanical Calculations. *J. Am. Chem. Soc.* **2001**, *222*, U403.
(46) Wang, J.; Wolf, R. M.; Caldwell, J. W.; Kollman, P. A.; Case, D. A. Development and Testing of a General Amber Force Field. *J. Comput. Chem.* **2004**, *25*, 1157–1174.
(47) Jakalian, A.; Jack, D. B.; Bayly, C. I. Fast, Efficient Generation of High‐quality Atomic Charges. AM1‐BCC Model: II. Parameterization and Validation. *J.*

Comp. Chem. **2002**, 23, 1623-1641.
(48) Rizzi, A.; Chodera, J.; Naden, L.; Beauchamp, K.; Albanese, S.; Grinaway, P.; Rustenburg, B.; Saladi, S.; Boehm, K. *Choderalab/yank: Bugfix Release*; **2018**.
(49) Horn, H. W.; Swope, W. C.; Pitera, J. W.; Madura, J. D.; Dick, T. J.; Hura, G. L.; Head-Gordon, T. Development of an Improved Four-Site Water Model for Biomolecular Simulations: TIP4P-Ew. *J. Chem. Phys.* **2004**, *120*, 9665–9678.
(50) Oliphant, T. E. SciPy: Open Source Scientific Tools for Python. *Comput. Sci. Eng.* **2007**, *9*, 10–20.
(51) Kraft, D. A Software Package for Sequential Quadratic Programming. *Forschungsbericht- Deutsche Forschungs- und Versuchsanstalt fur Luft- und Raumfahrt* **1988**.
(52) Reif, M. M.; Hünenberger, P. H. Computation of Methodology-Independent Single-Ion Solvation Properties from Molecular Simulations. III. Correction Terms for the Solvation Free Energies, Enthalpies, Entropies, Heat Capacities, Volumes, Compressibilities, and Expansivities of Solvated Ion. *J. Chem. Phys.* **2011**, *134*, 144103.
(53) Allen, F. H.; Kennard, O.; Watson, D. G.; Brammer, L.; Orpen, A. G.; Taylor, R. Tables of Bond Lengths Determined by X-Ray and Neutron Diffraction. Part 1. Bond Lengths in Organic Compounds. *J. Chem. Soc. Perkin Trans. 2.* **1987**, S1–S19.
(54) Irwin, B. W. J.; Huggins, D. J. Estimating Atomic Contributions to Hydration and Binding Using Free Energy Perturbation. *J. Chem. Theory Comput.* **2018**, *14*, 3218–3227.